Computational and Theoretical Chemistry 1046 (2014) 73–80

Contents lists available at ScienceDirect

Computational and Theoretical Chemistry

journal homepage: www.elsevier.com/locate/comptc

# Ab initio chemical kinetics for the $N_2H_4 + NO_x$ ($x = 1–3$) reactions and related reverse processes

P. Raghunath, Y.H. Lin, M.C. Lin *

*Center for Interdisciplinary Molecular Science, Department of Applied Chemistry, National Chiao Tung University, Hsinchu 300, Taiwan*

ARTICLE INFO

*Article history:*
Received 26 May 2014
Received in revised form 14 July 2014
Accepted 19 July 2014
Available online 29 July 2014

*Keywords:*
$N_2H_4$–$NO_x$ reactions
Thermochemistry
Kinetics and mechanisms

ABSTRACT

The kinetics and mechanisms for $N_2H_4 + NO_x$ ($x = 1–3$) reactions and the related reverse reactions have been investigated by ab initio molecular orbital theory based on the CCSD(T)/CBS//CCSD/6-31G(d,p), CCSD(T)//B3LYP and CCSD(T)//BH&HLYP methods with the 6-311++G(3df,2p) basis set. These reactions are important to the propulsion chemistry of the $N_2H_4$–$N_2O_4$ propellant system. The results show that the reactions of $N_2H_4$ with NO and $NO_2$ producing $N_2H_3$ + HNO and $N_2H_3$ + c-HONO by H-abstraction with 33.7 and 10.3 kcal/mol barriers, respectively, are dominant. For the $N_2H_4 + NO_3(D_{3h})$ reaction via two pre-reaction *van der* Waals complexes with 0.5 kcal/mol and −1.6 kcal/mol binding energies produces $HNO_3 + N_2H_3$ by H-abstraction and t-HONO + $N_2H_3O$ by concerted O- and H-atom transfers, respectively. The predicted enthalpies of formation of various products at 0 K are in good agreement with available experimental data within reported errors. Furthermore, the rate constants for the forward and some key reverse reactions have been predicted in the temperature range 300–2000 K with tunneling corrections using transition state theory (for direct abstraction) and variational Rice–Ramsperger–Kassel–Marcus theory (for association/decomposition) by solving the master equation.



## 1. Introduction

$N_2H_4$ and $NO_x$ ($x = 1–3$) co-exist in the early stages of the hydrazine-NTO ($N_2O_4$ nitrogen tetroxide) combustion reaction. The $NO_x$ species can be produced by the rapid dissociation $N_2O_4 \rightarrow 2NO_2$ followed by the disproportionation reaction, $2NO_2 \rightarrow NO + NO_3$. In addition, a large amount of NO can be generated by the very fast metathetical reaction of $NO_2$ with radicals such as H and $NH_2$ and $N_2H_3$, among others. Kinetics and mechanisms for the $N_2H_4 + NO_x$ reactions have not been experimentally investigated before by direct reagent or product detection [1]. A reliable characterization of these processes by a high-level ab initio chemical kinetic study is therefore called for.

Among the 3 reactions studied in the present work, the $NO_2 + N_2H_4$ reaction has been investigated by 3 research groups before. Sawyer and Glassman [2] studied the reaction in 1967 in an adiabatic flow reactor using a thermocouple to measure the rate of temperature rise. They attributed the T-rise to the initiation process which obeyed the kinetics: $-d[N_2H_4]/dt = k_2[NO_2][N_2H_4]$ with $k_2 = 10^{15.83}$ exp [−26,700/RT] $cm^3\ mol^{-1}\ s^{-1}$ (where $R = 1.987$ cal $mol^{-1}\ K^{-1}$), suggesting that the reaction $NO_2 + N_2H_4 \rightarrow HONO + N_2H_3$ has a very high barrier of 26.7 kcal $mol^{-1}$. More recently Lai et al. [3] reported the rate constant for the bimolecular reaction to be $k_2 = 3.23\ T^{3.56}$ exp(−384/T) $cm^3\ mol^{-1}\ s^{-1}$ from 250 to 2500 K temperature range based on the transition state theory (TST) calculation using the potential energy surface predicted with the G2M (CC3) method [4]. A similar ab initio chemical kinetic calculation employing the CBS-QB3 method by Koshi and coworkers [5], in their attempt to model the hypergolic reaction of NTO and hydrazine, gave rise to the expression $k_2 = 4.89 \times 10^1\ T^{3.43}$ exp(−5566/T) $cm^3\ mol^{-1}\ s^{-1}$ from 300 to 3000 K temperature. These data will be compared with our present results using a higher level of theory in conjunction with TST calculations.

The kinetics and mechanisms for both $N_2H_4$ reactions involving NO and $NO_3$ have not been studied before. The processes are believed to be intimately involved in the early stages of the hypergolic combustion of $N_2H_4$ and NTO because of the expected high concentrations of both $NO_x$ species, directly or indirectly through their reverse processes (such as $N_2H_3 + HNO \rightarrow N_2H_4 + NO$, $N_2H_3 + HONO \rightarrow N_2H_4 + NO_2$ and $N_2H_3 + HONO_2 \rightarrow N_2H_4 + NO_3$ at high temperatures). Parenthetically it should be mentioned that $HNO_3$ is one of the major products formed in the exothermic bimolecular initiation reaction, $N_2H_4 + ONONO_2 \rightarrow HNO_3 + H_2NHNO$ proposed by Lai et al. [3]. The results of the present calculations on the title reactions will be discussed in detail below.

* Corresponding author.
*E-mail address:* chemmcl@emory.edu (M.C. Lin).

http://dx.doi.org/10.1016/j.comptc.2014.07.011
2210-271X/

## 2. Computational methods

The mapping of the potential energy surfaces (PESs) of $N_2H_4$ + $NO_x$ ($x$ = 1–3) and some key reverse processes was carried out by using the Gaussian 09 program [6]. The geometries of the reactants, intermediates, transition states, and products of all the reactions were optimized with the CCSD/6-31G(d,p) [7], BH&HLYP/6-311++G(3df,2p) [8] and B3LYP/6-311++G(3df,2p) [9] methods. It should be mentioned that the ground state structure of the $NO_3$ radical predicted by some DFT methods such as BH&HLYP had $C_{2v}$ symmetry, which is inconsistent with the experimentally determined $D_{3h}$ structure [10]; accordingly, for the $NO_3$ reaction, we only used the geometries predicted by the CCSD method. Vibrational frequencies employed to characterize stationary points and zero-point vibrational energy (ZPVE) corrections were also calculated at the same levels of theory. For obtaining more accurate energies, we carried out higher level single-point energy calculations with extrapolation to the complete basis set (CBS) limit [11] using the CCSD/6-31G(d,p) optimized geometries for all 3 reactions. The CBS energies were evaluated with these geometries as follows. The total energies $E(X)$ computed with the cc-PVXZ basis sets ($X$ = 2, 3, 4) extrapolated to the CBS limits $E_{CBS}$ employing a three-point extrapolation scheme [11],

$$E(X) = E_{CBS} + b\,\exp[-(X-1)] + c\,\exp[-(X-1)^2]$$

where $E(X)$ is the single point energy calculated by CCSD(T)/cc-pVXZ method [12], $X$ is the cardinal number of the basis sets connected with $X$ = 2 (DZ), 3 (TZ), 4 (QZ) and $E_{CBS}$, $b$, and $c$ are parameters to be fitted. In addition, we also carried out single point energy calculations by the CCSD(T)/6-311++G(3df,2p) method [7] using the DFT optimized geometries for NO and $NO_2$ reactions. Rate constant predictions for all forward reactions were based on the CBS-limit values using the CCSD/6-31G(d,p) optimized geometries; whereas for some key reverse processes of the NO and $NO_2$ reactions, their rate constants were predicted with the CCSD(T)/6-311++G(3df,2p)//BH&HLYP/6-311++G(3df,2p) energies.

The rate constants were calculated using the microcanonical transition-state theory (TST) and/or the Rice–Ramsperger–Kassel–Marcus (RRKM) theory by solving the one-dimensional master equation to derive the nonequilibrium distribution function for each channel with the VARIFLEX program suite [13]. For a barrierless dissociation process, the Morse function, $V(R) = D_e\{1-\exp[-\beta(R-R_e)]\}^2$, was employed to fit the dissociation energy curve and approximate the minimum energy path (MEP) for the rate constant calculation. In the Morse function, $R$ is the reaction coordinate (i.e., the distance between two bonding atoms), $R_e$ is the equilibrium value of $R$, and $D_e$ is the binding energy excluding zero-point energy. For tight transition states, the numbers of states were evaluated according to the rigid-rotor harmonic-oscillator assumption [13].

## 3. Results and discussions

### 3.1. Potential energy surfaces and reaction mechanisms

The equilibrium geometries of various species involved in the reactions computed at the CCSD/6-31G(d,p) level are summarized in Fig. 1. For the NO and $NO_2$ reactions, the structures predicted with the BH&HLYP/6-311++G(3df,2p) method are very similar. The potential energy surfaces (PES's) of the 3 $N_2H_4$ reactions were predicted at the CBS//CCSD/6-31G(d,p) + ZPVE level of theory; the results are presented in Fig. 2. Additionally, the results for $N_2H_4$ reactions with NO and $NO_2$ obtained by different methods have been compared in Table 1 and 2. In this work, we also study the reverse reaction mechanisms of $N_2H_3$ with HNO and HONO at the CCSD(T)//BH&HLYP/6-311++G(3df,2p) level as shown in Fig. 3. The moments of inertia and the vibrational frequencies of all the species involved in these reactions are listed in Tables S1 and S2 for the kinetic calculations. The calculated heats of formation of major species at 0 K are compared with experimental data in Table 3. The following discussion will be based on the energies computed at the CBS//CCSD/6-31G(d,p) level unless specified otherwise, and all the energies of TS's and intermediates cited are relative to the reactants.

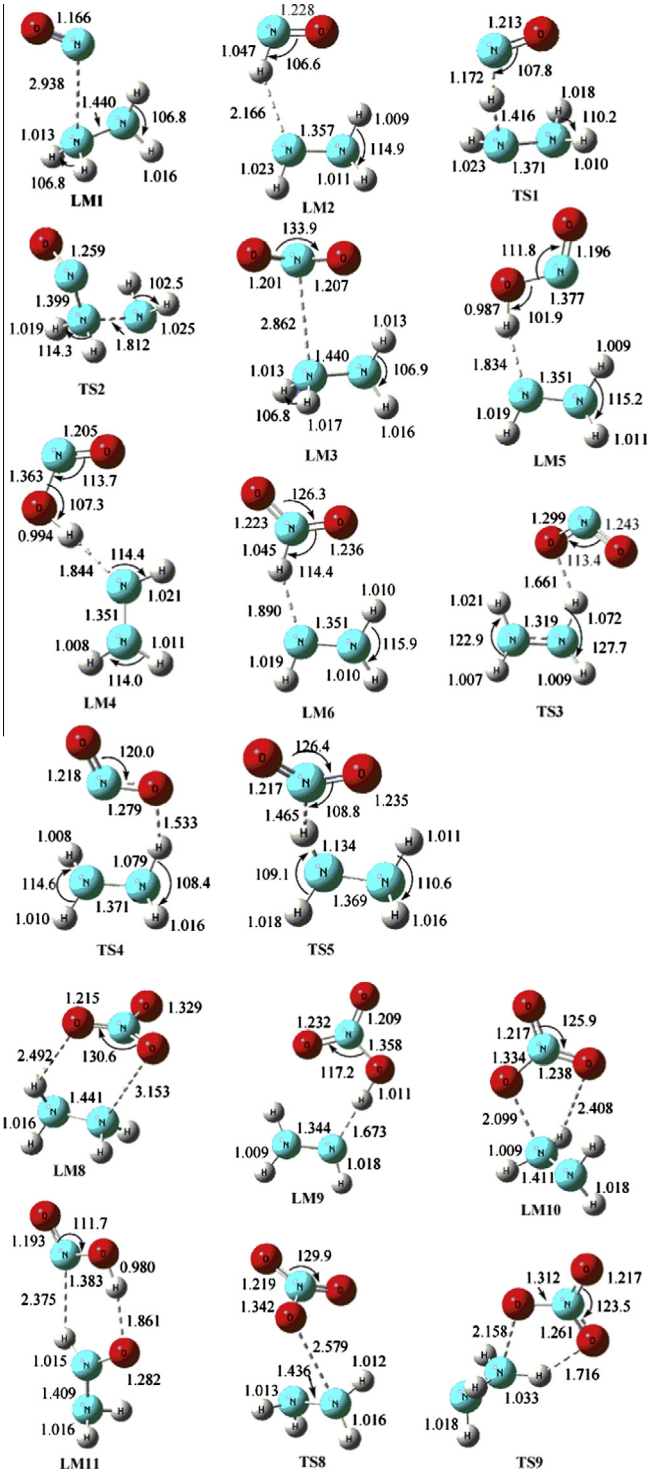


**Fig. 1.** The optimized geometries of the reactants, intermediates, transition states and products computed at the CCSD/6-31G(d,p) level (length in Å and angle in degree).

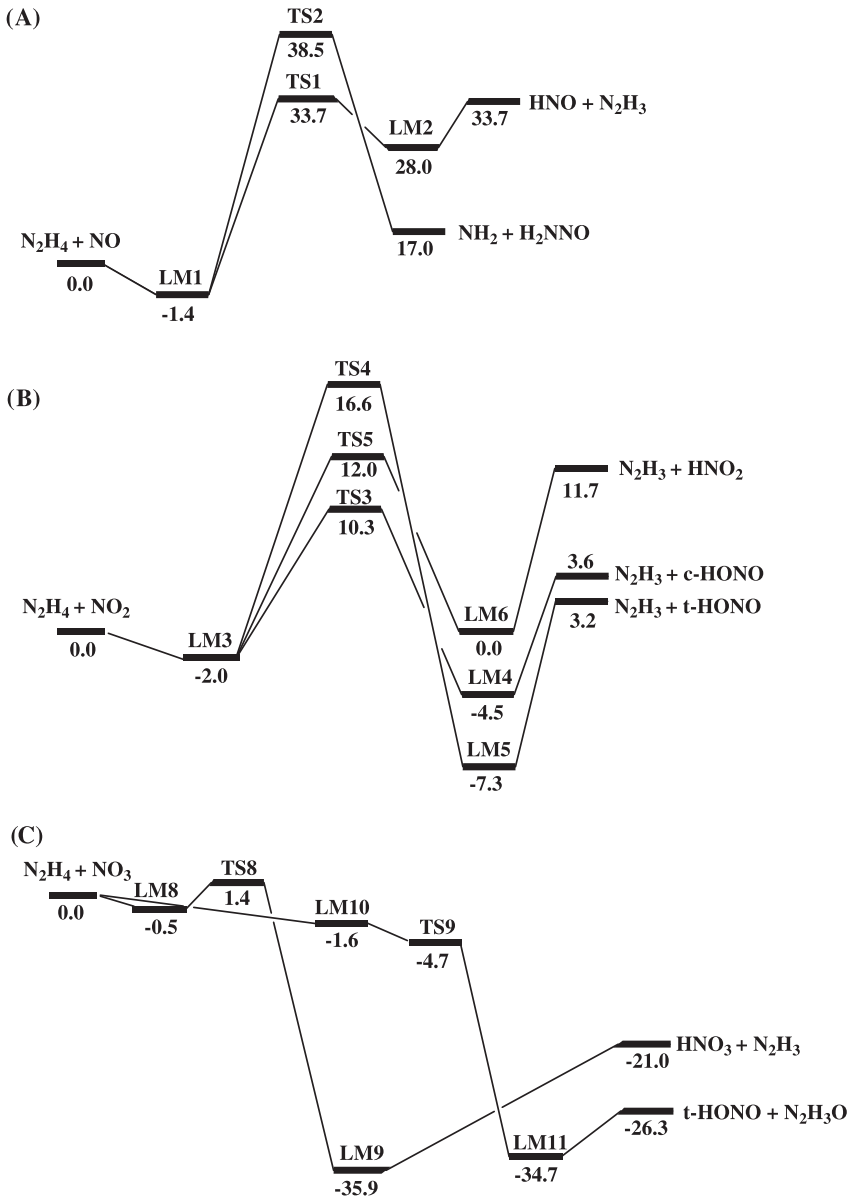


**Fig. 2.** Schematic energy diagram for $N_2H_4$ reactions with $NO_x$ ($x$ = 1–3) computed at the CCSD(T)/CBS//CCSD/6-31G(d,p) level with ZPVE corrections. Relative energies are given in kcal/mol at 0 K.

**Table 1**
The energies of species for $N_2H_4$ + NO computed at the various levels of theory with ZPVE corrections. Relative energies are given in kcal/mol.

| Species | CCSD(T)/6-311++G(3df,2p) | | CCSD(T)/CBS //CCSD |
|---|---|---|---|
| | BH&HLYP | B3LYP | |
| $N_2H_4$ + NO | 0.0 | 0.0 | 0.0 |
| LM1 | −1.6 | −1.4 | −1.4 |
| LM2 | 28.0 | 27.9 | 28.0 |
| TS1 | 33.7 | 35.1 | 33.7 |
| TS2 | 39.1 | 38.9 | 38.5 |
| HNO + $N_2H_3$ | 33.7 | 33.7 | 33.6 |
| $NH_2$ + $H_2NNO$ | 17.5 | 17.7 | 17.0 |

### 3.1.1. Reactions of $N_2H_4$ + NO

We have carried out an exhaustive search for the potential energy paths and mechanism of the $N_2H_4$ + NO reaction as shown in Fig. 2A. As revealed by the PES, there are two possible reaction paths: H abstraction and substitution reactions. Both the product channels proceed via a loose pre-reaction complex formed by the nitrogen of NO bonding with one of the nitrogen of the $N_2H_4$ forming the LM1 complex with 1.6 kcal/mol binding energy. The bond length of N···N complex is 2.938 Å. Firstly, the intermediate LM1 can react via the lowest energy channel by NO attacking on one of the hydrogen atoms in $N_2H_4$ through TS1 to yield the HNO + $N_2H_3$ via the post-reaction complex HNO:$N_2H_3$, LM2, with a barrier of 33.7 kcal/mol; the CBS/CCSD value is very close to the values obtained by the CCSD(T)//BH&HLYP and CCSD(T)//B3LYP methods with the 6-311++G(3df,2p) basis set, 33.7 and 35.1, respectively (see Table 1). The endothermicity of this process predicted by CCSD(T)/BH&HLYP and that by the CBS extrapolation, 33.7 and 33.6 kcal/mol, respectively, are in close agreement with the experimental value, 33.0 kcal/mol [14,15]. In the second mechanism, the reaction takes place by the attack of the nitrogen of NO at one of the nitrogen atoms of $N_2H_4$ via TS2 to give $NH_2$ + $H_2NNO$. The reaction barrier is 38.5 kcal/mol, which is 4.8 kcal/mol higher than TS1. Furthermore, the endothermicity of this process is computed to be 17.0 kcal/mol. The reaction barriers and the heats of reaction

**Table 2**
The energies of species for $N_2H_4 + NO_2$ computed at the various levels of theory with ZPVE corrections. Relative energies are given in kcal/mol.

| Species | CCSD(T)/6-311++G(3df,2p) | | G2M(CC1)[3] | CBS-QB3[5] | CCSD(T)/CBS//CCSD |
|---|---|---|---|---|---|
| | BH&HLYP | B3LYP | | | |
| $N_2H_4 + NO_2$ | 0.0 | 0.0 | 0.0 | 0.0 | 0.0 |
| LM3 | −2.6 | −3.6 | −2.5 | −1.9 | −2.0 |
| LM4 | −5.1 | −6.1 | −4.9 | – | −4.5 |
| LM5 | −7.5 | −8.3 | −7.6 | −6.9 | −7.3 |
| LM6 | −0.4 | −1.1 | −0.5 | −0.3 | 0.0 |
| TS3 | 10.5 | 7.7 | 7.6 | – | 10.3 |
| TS4 | 16.4 | 15.6 | 13.0 | 12.8 | 16.6 |
| TS5 | 12.8 | 10.4 | 9.4 | 9.3 | 12.0 |
| $N_2H_3$ + c-HONO | 3.5 | 3.4 | 3.4 | – | 3.6 |
| $N_2H_3$ + t-HONO | 3.2 | 3.9 | 2.9 | 4.0 | 3.2 |
| $N_2H_3 + HNO_2$ | 11.5 | 12.6 | 11.3 | 12.0 | 11.7 |

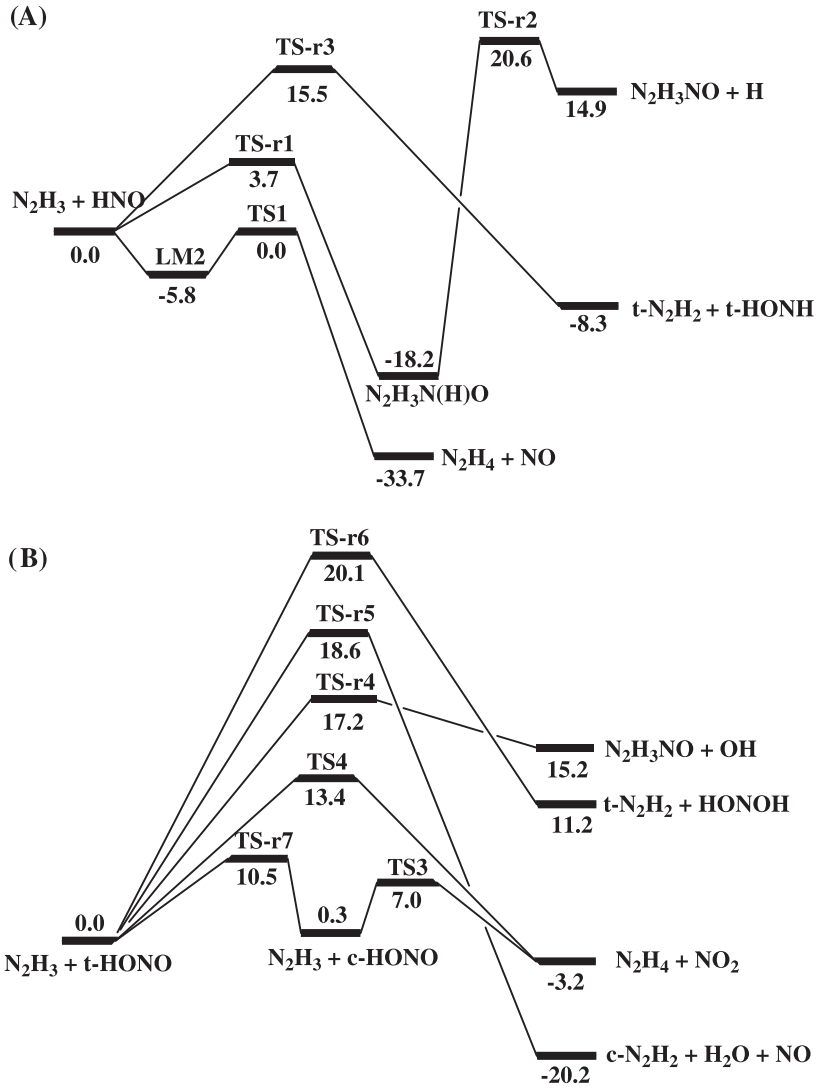


**Fig. 3.** Schematic energy diagram for the reverse processes of $N_2H_3$ with HNO and HONO computed with the CCSD(T)//BH&HLYP method employing the 6-311++G(3df,2p) basis set with ZPVE corrections. Relative energies are given in kcal/mol at 0 K.

predicted by the 3 methods agree within 1.5 kcal/mol for the worst case.

### 3.1.2. Reactions of $N_2H_4 + NO_2$

The potential energy diagram obtained at the CBS//CCSD/6-31G(d,p) level and their optimized geometries computed with the CCSD/6-31G(d,p) method are presented in Figs. 2B and 1, respectively. The relative energies of all the H-abstraction reaction channels obtained at different levels of theory are listed in Table 2 including the G2M(CC1) and CBS-QB3 results obtained by Lai et al. [3] and Daimon et al. [5], respectively. Comparison of these data will be made below for the individual channels discussed. As shown in the PES, there are three H-abstraction and one association channel. All the H-abstraction channels take place via the pre-reaction complex, LM3 ($O_2N\cdots NH_2–NH_2$), at a separation of 2.862 Å between the $NO_2$ and $N_2H_4$ with 2.0 kcal/mol binding

**Table 3**
Heats of formation ($\Delta_f H_0°$) of product species at 0 K predicted by CCSD(T)/CBS//CCSD/6-31G(d,p) given in kcal/mol. Values in parentheses are predicted by CCSD(T)//BH&HLYP/6-311++G(3df/2p).

| Species | Reactions | Heat of formation $\Delta_f H_0°$ | |
|---|---|---|---|
| | | Calculated | Literature[a] |
| $N_2H_3$ | $N_2H_4 + NO \rightarrow HNO + N_2H_3$ | 56.8 (56.9) | 56.2 |
| $H_2NNO$ | $N_2H_4 + NO \rightarrow NH_2 + H_2NNO$ | 19.5 (20.0) | 20.0 |
| $HNO_2$ | $N_2H_4 + NO_2 \rightarrow N_2H_3 + HNO_2$ | −9.7 (−9.9) | – |
| c-HONO | $N_2H_4 + NO_2 \rightarrow N_2H_3$ + c-HONO | −17.8 (−17.9) | −16.9 ± 0.3 |
| t-HONO | $N_2H_4 + NO_2 \rightarrow N_2H_3$ + t-HONO | −18.2 (−18.2) | −17.4 ± 0.3 |
| $HNO_3$ | $N_2H_4 + NO_3 \rightarrow N_2H_3 + HNO_3$ | −32.1 | −29.8 ± 0.1 |
| $N_2H_3O$ | $N_2H_4 + NO_3 \rightarrow$ t-HONO + $N_2H_3O$ | −37.8 | 37.7 ± 0.2 |

[a] The experimental values utilized in the calculations are obtained based on the enthalpies of formation at 0 K for $N_2H_4$ = 26.2 kcal/mol; NO = 21.5 ± 0.1 kcal/mol; $NO_2$ = 8.6 ± 0.2 kcal/mol; HNO = 24.5 kcal/mol; $NO_3$ = 18.9 kcal/mol; $HNO_3$ = −29.8 ± 0.1 kcal/mol; t-HONO = −17.4 ± 0.3 kcal/mol; c-HONO = −16.9 ± 0.3 kcal/mol (Ref. [14]); $N_2H_3$ = 56.2 kcal/mol (Ref. [15]); $NH_2$ = 45.2 ± 0.24 kcal/mol (Ref. [17]); $N_2H_3O$ = 37.7 ± 0.2 kcal/mol and $H_2NNO$ = 20.0 kcal/mol (Ref. [1]).

energy. The first low energy barrier products are $N_2H_3$ + cis-HONO, formed by one of the oxygen atoms in the $NO_2$ abstracting an H atom from $N_2H_4$ via transition state TS3 with a barrier of 10.3 kcal/mol, yielding a product complex, LM4 ($ONOH\cdots NHNH_2$), with the exothermicity of 4.5 kcal/mol. LM4 dissociates further to $N_2H_3$ + cis-HONO with the dissociation energy of 8.1 kcal/mol. The barrier height of this reaction is 2.7 kcal/mol higher than the value 7.6 kcal/mol calculated at the G2M(CC1)//B3LYP/6-311++G(3df,2p) level by Lai et al. [3]. The latter is, however, close to the value, 7.5 kcal/mol, predicted by the CCSD(T)/6-311++G(3df,2p) //B3LYP/6-311++G(3df,2p) method. At the CCSD(T)//BH&HLYP level, the barrier was found to be 10.5 kcal/mol, in close agreement with the CBS//CCSD/6-31G(d,p) result. In the second product channel producing $N_2H_3$ + trans-HONO, one of the oxygen atoms in $NO_2$ abstracts one of H atoms of $N_2H_4$ via a trans-position through TS4 which requires a 16.6 kcal/mol barrier energy via the LM5 complex. This value is 3.6 and 3.8 kcal/mol higher than those predicted by Lai et al. [3] and Daimon et al. [5], respectively. To summarize both abstraction results, the formation of cis-HONO requires 6.3 kcal/mol lower energy barrier, when compared to the production of trans-HONO. As shown in Fig. 2B, the next low-energy H-abstraction product channel produces $N_2H_3 + HNO_2$ occurring by the abstraction by the central N atom of the $NO_2$ one of H atoms in $N_2H_4$ via TS5 with 12.0 kcal/mol energy.

Lastly, we studied the production of $H_2NN(O)H_2$ + NO which occurs by the association of one of O atoms in $NO_2$ with one of N atoms in $N_2H_4$ via TS6 with a high barrier of 44.8 kcal/mol, forming a product complex, LM7, with the endothermicity of 16.6 kcal/mol calculated by the CCSD(T)//BH&HLYP method; see Fig. S2 of Supporting Information. The intermediate LM7 dissociates to give $H_2NN(O)H_2$ + NO with the dissociation energy of 2.4 kcal/mol. The $H_2NN(O)H_2$ radical can undergo further H migration involving one of the vicinal H atoms attaching to the N atom to the O atom giving $H_2NN(H)OH$. This process has a high energy barrier (47.8 kcal/mol) via TS7 with an overall exothermicity computed to be 1.2 kcal/mol. As shown in Table 2, the transition state energies predicted at the CBS//CCSD level are close to those computed by the CCSD//BH&HLYP method. The results obtained by CCSD//B3LYP, G2M(CC1) and CBS-QB3 methods are about 3.0 kcal/mol lower, essentially resulted from the looser TS structures predicted by the B3LYP method. The barrier height at TS3 predicted by B3LYP/6-311++G(3df,2p) was found to be as low as 2.4 kcal/mol, which may be compared with the values predicted by BH&HLYP/6-311++G(3df,2p) and CCSD/6-31G(d,p), 8.6 and 9.5 kcal/mol, respectively, which are much closer to the CBS result of 10.3 kcal/mol.

### 3.1.3. Reactions of $N_2H_4 + NO_3$

For this reaction system, we employed the CCSD(T)/CBS//CCSD/6-31G(d,p) method for PES mapping as some DFT methods such as BH&HLYP and others alluded to below failed to predict the ground state structure of the $NO_3$ radical as aforementioned. Previously, Wille et al. [16] studied $NO_3$ reactions with alkynes using various DFT methods: B3LYP, BH&HLYP, mPW1PW91 and mPW1K. They reported that $NO_3$ with the $C_{2v}$ symmetry geometry is more stable by the BH&HLYP, mPW1PW91 and mPW1K methods, whereas the $D_{3h}$ symmetry geometry is more stable with B3LYP. The results by BH&HLYP/cc-pVDZ were found to be in good agreement with those of QCISD and CCSD(T) methods. In the present case, however, the B3LYP method failed to predict the existence of the pre-reaction complexes for the $N_2H_4 + NO_3$ reaction. In the present reaction, $D_{3h}$ symmetry has been considered for the $NO_3$ radical, to be consistent with experimental data. The N–O bond length in $NO_3$ with the $D_{3h}$ symmetry is 1.238 Å calculated by CCSD/6-31G(d,p) which is in close agreement with the experimental value of 1.240 Å [10].

In this reaction, there are two possible low energy channels via pre-reaction complexes computed with the CCSD(T)/CBS//CCSD/6-31G(d,p) method as shown in Fig. 2C; their related optimized structures are given in Fig. 1. In the first channel producing t-HONO + $N_2H_3O$, the reaction proceeds via the van der Waals complex, $N_2H_4$:$NO_3$ (LM8) with 0.5 kcal/mol binding energy. The pre-reaction complex can further readily isomerize by H-abstraction from one of the N–H bonds in $N_2H_4$ via TS8, with 1.4 kcal/mol barrier above the reactants to produce the post-reaction complex, $N_2H_3 + HNO_3$ (LM9). The process is exothermic by 35.9 kcal/mol at the CBS//CCSD level; LM9 can easily decompose to produce $N_2H_3 + HNO_3$ (at −21.0 kcal/mol) with no intrinsic TS. As shown in Fig. 2C, the second reaction occurs via the pre-reaction complex LM10 with 1.6 kcal/mol binding energy in which one of the O atoms of $NO_3$ interacting with one of the N atoms in $N_2H_4$ by a barrierless process. As the reaction proceeds, the LM10 can dissociate further by the transfer of an H atom from $N_2H_4$ to a neighboring O atom in $NO_3$ with the concerted transfer of another O atom to $N_2H_3$ via the five-membered ring low-energy TS9 with the negative activation barrier of 3.1 kcal/mol to form a product complex, LM11. Further dissociation the reaction produces $N_2H_3O$ + t-HONO with 26.3 kcal/mol exothermicity. In this potential energy surface, the reactions LM8 → $N_2H_4 + NO_3$, LM9 → $N_2H_3 + HNO_3$, LM10 → $N_2H_4 + NO_3$ and LM11 → t-HONO + $N_2H_3O$ have no well-defined intrinsic transition states; their association/dissociation potential functions, computed variationally to their separate products at the DFT level, are fitted to the Morse functions with $\beta$ = 1.40 Å$^{-1}$, $\beta$ = 1.35 Å$^{-1}$, $\beta$ = 1.82 Å$^{-1}$ and $\beta$ = 1.13 Å$^{-1}$ respectively. These values will be used in the rate constant calculations to be discussed below. It is worth noting that the PES for the exothermic reaction of the nitrate radical is quite similar to those of analogous exothermic reactions of $NH_3$ with chlorate ($ClO_3$) and perchlorate ($ClO_4$) radicals [17].

### 3.2. Reverse reaction mechanisms of $N_2H_3$ with HNO and HONO

The low-energy products, $N_2H_3$, HNO and HONO formed in the $N_2H_4$ reactions with NO and $NO_2$ may co-exist in the hydrazine-NTO combustion system. Considering the important role of these species, we studied the reverse reactions in which many new reaction channels inaccessible to the forward processes are open with relatively low reverse barriers. As presented in previous sections, the results from both DFT and CCSD(T)/CBS//CCSD methods appear to agree closely in geometries and relative energies for the reactions of $N_2H_4$ with NO and $NO_2$. The PES's of the reverse reactions of $N_2H_3$ with HNO and HONO were predicted only by using the CCSD(T)//BH&HLYP method with the 6-311++G(3df,2p) basis set as shown in Fig. 3 and their geometrical parameters are shown

in Fig. S2. As discussed in Fig. 2A, the $N_2H_4$ + NO reaction produces $N_2H_3$ + HNO with the lowest energy barrier. Similarly in the reverse reaction of $N_2H_3$ + HNO, the $N_2H_4$ + NO reaction is also the lowest energy process. Another product pair, $N_2H_3NO$ and H, can be formed from the $N_2H_3$ + HNO reaction via association process yielding the $N_2H_3N(H)O$ intermediate with the energy barrier of 3.7 kcal/mol(TS-r1). However, the elimination of the H atom requires a high energy barrier of 20.6 kcal/mol at TS-r2. On this PES, the next low energy product channel gives t-$N_2H_2$ + t-HONH occurring by direct H-abstraction via TS-r3 with 15.5 kcal/mol barrier energy.

#### 3.2.1. $N_2H_3$ + HONO

As discussed above, $N_2H_3$ + HONO are the low-energy products in the $N_2H_4$ + $NO_2$ reaction. HONO molecule possesses two stable geometrical conformers in the gas phase: *cis* and *trans*. The *trans*-conformer is 0.3 kcal/mol more stable than the *cis*-conformer. The barrier energy for *trans* to *cis*-conformation is 10.5 kcal/mol (TS-r7) calculated by the CBS//CCSD method (see Fig. 3B). For the reverse processes, we calculated major low energy product channels from $N_2H_3$ + c-/t-HONO by CCSD(T)//BH&HLYP; the PES is presented in Fig. 3B. The calculation of $N_2H_3$ + c-HONO reaction shows that the direct hydrogen abstraction occurred by the attack of H atom of c-HONO at the N atom of the NH group in $N_2H_3$ produces the $N_2H_4$ + $NO_2$ *via* TS3 with a 6.7 kcal/mol barrier energy at the CBS//CCSD level. Similarly, we also calculated for the barrier energy of the $N_2H_3$ + t-HONO reaction channel producing $N_2H_4$ + $NO_2$ to be 13.4 kcal/mol. Based on our results the reverse reaction of $N_2H_3$ with *cis*- and *trans*-HONO producing $N_2H_4$ + $NO_2$ have the lowest energy barriers. The next pathway of the lower energy reaction occurs by the attack of the N atom of the NH group of $N_2H_3$ at the N atom of HONO via TS-r4 with 17.2 kcal/mol barrier energy, according to CCSD(T)//BH&HLYP, producing $N_2H_3NO$ + OH products. The next low-energy channel involves the interaction of the HO group of HONO with one of the H atoms of the $NH_2$ group in $N_2H_3$ leading to the formation of c-$N_2H_2$ + $H_2O$ + NO with 18.6 kcal/mol barrier at TS-r5. Finally, H-abstraction from the $NH_2$ group of $N_2H_3$ by the terminal O atom of HONO via TS-r6 with 20.1 kcal/mol barrier energy producing t-$N_2H_2$ + HONOH with an overall endothermicity of 11.2 kcal/mol. The rate constants for these reverse processes have been computed and reported below.

### 3.3. Enthalpies of formation

The predicted heats of formation of most product species involved in the $N_2H_4$ + $NO_x$ ($x$ = 1–3) reactions are presented in Table 3 based on the energies computed at the CBS//CCSD/6-31G(d,p) and CCSD(T)//BH&HLYP/6-311++G(3df,2p) levels. The heats of formation were determined by combining the computed heats of reaction ($\Delta_r H_0^\circ$) based on the CBS-limit values and CCSD(T)//BH&HLYP with the experimental heats of formation ($\Delta_f H_0^\circ$) of other known species involved in the reaction at 0 K [14,15,18]. With the experimental heats of formation referenced in the footnote of Table 3, we obtained the values at 0 K for $N_2H_3$, c-HONO and t-HONO to be 56.8, −17.8 and −18.2 kcal/mol, respectively, with an estimated error of ±1.2 kcal/mol. The predicted heats of formation of these and other products are listed in Table 3 for comparison with available data in the literature; in general, the agreement is quite good.

### 3.4. Rate constant calculations

The predicted rate constants for all the low-energy product channels of $N_2H_4$ + $NO_x$ ($x$ = 1–3) are summarized below:

$$N_2H_4 + NO \rightarrow N_2H_3 + HNO \quad (1)$$

$$\rightarrow NH_2 + H_2NNO \quad (2)$$

$$N_2H_4 + NO_2 \rightarrow N_2H_3 + \text{c-HONO} \quad (3)$$

$$\rightarrow N_2H_3 + HNO_2 \quad (4)$$

$$\rightarrow N_2H_3 + \text{t-HONO} \quad (5)$$

$$N_2H_4 + NO_3 \rightarrow N_2H_3 + HNO_3 \quad (6)$$

$$\rightarrow \text{t-HONO} + N_2H_3O \quad (7)$$

The rate constants for the forward reactions of $N_2H_4$ + $NO_x$ ($x$ = 1–2) channels using the transition state theory (TST) [19] with Eckart tunneling corrections [20] have been computed in the temperature range of 300–2000 K with the Variflex code [13], whereas the higher energy H-production channels are neglected. Rate constants are calculated according to the predicted PES's as shown in Fig. 2 using energies obtained at the CCSD(T)/CBS//CCSD level and the moment of inertia and harmonic vibrational frequencies obtained by the CCSD/6-31G(d,p) presented in Table S1 in Supporting Information.

The Arrhenius plots for the $N_2H_4$ + NO reaction product rate constants of reactions (1) and (2) are presented in Fig. 4. The three-parameter fits in the 300–2000 K temperature range give the following expression in $cm^3$ $molecule^{-1}$ $s^{-1}$:

$$k_1 = 1.07 \times 10^{-22} T^{3.16} \exp(-15342/T)$$
$$k_2 = 8.35 \times 10^{-23} T^{2.98} \exp(-17919/T)$$

The rate constants for the H-abstraction reactions of $N_2H_4$ with $NO_2$ forming various products $k_3$–$k_5$ are predicted in the temperature range of 300–2000 K and compared with the available computed results as shown in Fig. 5. It is evident that H-abstraction producing c-HONO via TS3 is predominant comparing with other two abstraction reactions. The three-parameter fits in the 300–2000 K temperature range given in the unit of $cm^3$ $molecule^{-1}$ $s^{-1}$ for reactions (3)–(5) are given below along with previous computed results:

$$k_3 = 1.37 \times 10^{-22} T^{3.13} \exp(-4460/T)$$
$$k_3 = 3.20 \times 10^{-25} T^{3.74} \exp(-1663/T) \text{ (Ref. [3])}$$
$$k_4 = 4.00 \times 10^{-26} T^{4.14} \exp(-3999/T)$$
$$k_5 = 5.45 \times 10^{-26} T^{4.00} \exp(-6500/T)$$

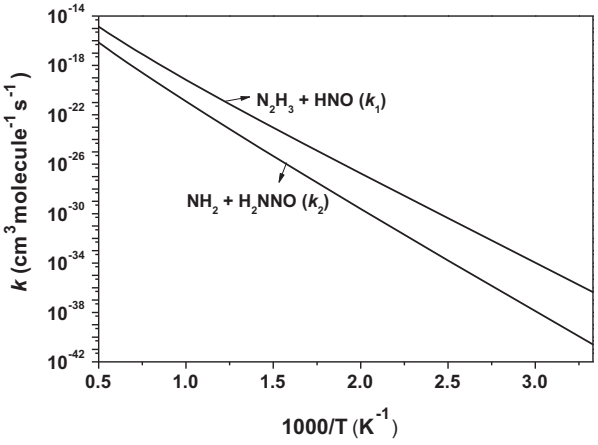


**Fig. 4.** The predicted rate constants for the $N_2H_4$ + NO reaction forming $N_2H_3$ + HNO ($k_1$) and $NH_2$ + $H_2NNO$ ($k_2$) based on the CCSD(T)/CBS//CCSD/6-31G(d,p) results.

$k_5 = 8.12 \times 10^{-23} T^{3.43} \exp(-5566/T)$ (Ref. [5])

The recent result of $N_2H_4 + NO_2 \rightarrow$ c-HONO + $N_2H_3$ ($k_3$) calculated by Lai et al. [3] with the G2M//B3LYP method is also shown in Fig. 5. The result is found to be 3 order magnitudes higher at low temperatures because of their smaller barrier energy at TS3 (2.7 kcal/mol lower than that by the CCSD(T)/CBS//CCSD method). Our predicted rate constant $k_5$ for t-HONO formation is lower than the value reported by Daimon et al. [5], attributable to our higher barrier energy at TS4, 16.6 kcal/mol, than their 12.8 kcal/mol. We have also carried out rate constant calculations using the CCSD(T)/BH&HLYP values for the $N_2H_4 + NO_x$ ($x = 1$–2) and compared with those by CBS//CCSD/6-31G(d,p) as shown in Supporting Information Figs. S3 and S4. All the calculations at the CCSD(T)/BH&HLYP level of theory are in good accord with those by the CBS//CCSD/6-31G(d,p) method.

The rate constants for the $N_2H_4 + NO_3$ reaction product channels are calculated by variational TST and RRKM rate theory using the energetics presented in Fig. 2C along with Morse potential energies and the vibrational frequencies and rotational constants are displayed in Table S1. The VTST calculations were carried out with the unified statistical formulation of Miller [21] including multiple reflection corrections [22] above the shallow wells of the pre-reaction and post-reaction complexes. The Lennard-Jones parameters for collision rate estimates are obtained by using $\sigma = 3.85$ Å and $\varepsilon = 153.4$ K for $N_2H_4$:$NO_3$, derived from those of $N_2H_4$ ($\sigma = 4.23$ Å and $\varepsilon = 205$ K) and $NO_3$ ($\sigma = 3.462$ Å and $\varepsilon = 114.8$ K) and $N_2H_4$ buffer gas [23]. The predicted rate constant for the both product channels $N_2H_3 + HNO_3$ ($k_6$) and t-HONO + $N_2H_3O$ ($k_7$) are pressure-independent at <100 atm, as shown in Fig. 6 given by the following expressions in the units of $cm^3$ molecule$^{-1}$ $s^{-1}$ in the different temperature ranges:

$$k_6 = 1.03 \times 10^{-20} T^{2.64} \exp(-299/T) \quad (300\text{–}2000\ \text{K})$$
$$k_7 = 2.70 \times 10^{-13} T^{0.20} \exp(1097/T) \quad (300\text{–}1000\ \text{K})$$
$$= 3.38 \times 10^{-21} T^{2.59} \exp(2824/T) \quad (1000\text{–}2000\ \text{K})$$

*3.4.1. Reverse reaction rate constants*

As shown in the PES (Fig. 3), the reverse reactions of $N_2H_3$ with HNO and HONO can occur through many product channels as shown below.

$$N_2H_3 + HNO \rightarrow N_2H_4 + NO \quad (8)$$

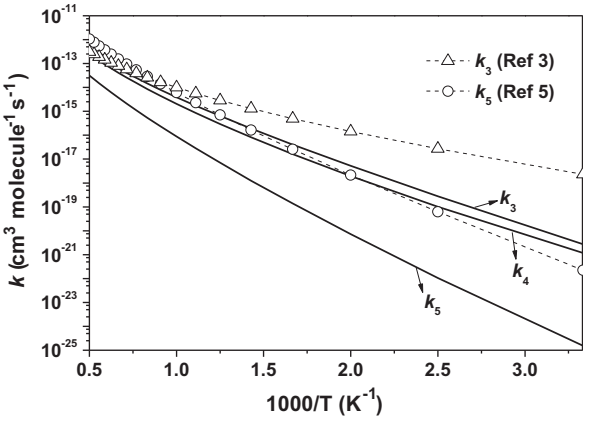


**Fig. 5.** The predicted rate constants for the $N_2H_4 + NO_2$ reaction forming $N_2H_3$ + c-HONO ($k_3$), $N_2H_3 + HNO_2$ ($k_4$) and $N_2H_3$ + t-HONO ($k_5$) based on the CCSD(T)/CBS//CCSD/6-31G(d,p) results, comparing with the data of Lai et al. [3] and Daimon et al. [5].

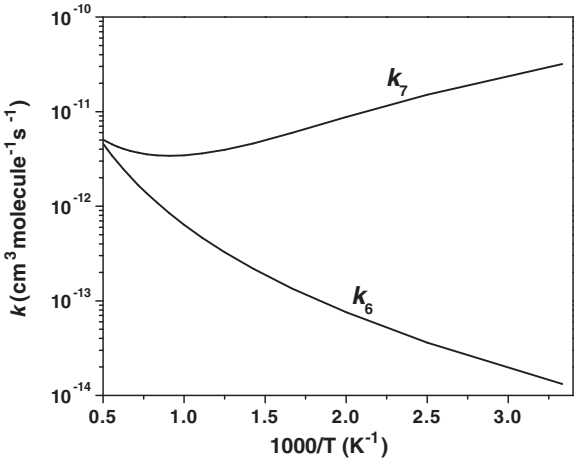


**Fig. 6.** Predicted rate constants for the $N_2H_4 + NO_3$ reaction forming $N_2H_3 + HNO_3$ ($k_6$) and t-HONO + $N_2H_3O$ ($k_7$) based on the CCSD(T)/CBS//CCSD/6-31G(d,p) results.

$$\rightarrow N_2H_3NO + H \quad (9)$$

$$\rightarrow \text{t-}N_2H_2 + \text{t-HONH} \quad (10)$$

$$N_2H_3 + \text{t-HONO} \rightarrow N_2H_3NO + OH \quad (11)$$

$$\rightarrow \text{c-}N_2H_2 + H_2O + NO \quad (12)$$

$$N_2H_3 + \text{c-HONO} \rightarrow N_2H_4 + NO_2 \quad (13)$$

$$N_2H_3 + \text{t} - \text{HONO} \rightarrow N_2H_4 + NO_2 \quad (14)$$

Rate constants for all these product channels have been calculated by the transition state theory (TST) with Eckart tunneling corrections, employed in the Variflex [13]. For the rate constant calculations, we used the CCSD(T)//BH&HLYP barrier heights and the BH&HLYP/ 6-311++G(3df,2p) molecular parameters of the reactants and transition states which are presented in Table S2. The calculated rate constant expressions for all the reaction channels R8-R13 obtained by three-parameter fitting for the 300–2000 K temperature range are given below,

$$k_8 = 1.05 \times 10^{-20} T^{2.14} \exp(1254/T) \quad (300\text{–}600\ \text{K})$$
$$= 1.61 \times 10^{-25} T^{3.67} \exp(2017/T) \quad (600\text{–}2000\ \text{K})$$
$$k_9 = 2.74 \times 10^{-26} T^{3.82} \exp(-8947/T) \quad (300\text{–}2000\ \text{K})$$
$$k_{10} = 8.06 \times 10^{-41} T^{8.15} \exp(455/T) \quad (300\text{–}2000\ \text{K})$$
$$k_{11} = 7.78 \times 10^{-24} T^{2.94} \exp(-7739/T) \quad (400\text{–}2000\ \text{K})$$
$$k_{12} = 4.64 \times 10^{-32} T^{5.51} \exp(-5592/T) \quad (400\text{–}2000\ \text{K})$$
$$k_{13} = 1.15 \times 10^{-21} T^{2.57} \exp(-2838/T) \quad (300\text{–}2000\ \text{K})$$
$$k_{14} = 8.95 \times 10^{-26} T^{3.64} \exp(-5088/T) \quad (300\text{–}2000\ \text{K}).$$

## 4. Conclusion

The kinetics and mechanisms for a series of reactions of $N_2H_4$ with $NO_x$ ($x = 1$–3) radicals and its reverse reactions have been studied at the CCSD(T)/CBS//CCSD/6-31G(d,p) level of theory for all 3 systems and with additional two DFT based methods, CCSD(T)//B3LYP/6-311++G(3df,2p) and CCSD(T)//BH&HLYP/6-311++G(3df,2p) for NO and $NO_2$ reactions and some of their key reverse processes, in conjunction with RRKM and TST calculations. The results of these calculations show that the H-abstraction process is the most favorable low-energy reaction channel in each of these reactions. The predicted barriers for $N_2H_4$ with NO and $NO_2$ reactions are 33.7 kcal/mol and 10.3 kcal/mol, respectively, for the formation of $N_2H_3$ + HNO and $N_2H_3$ + c-HONO products. In the case of $N_2H_4 + NO_3$, the results show that the reaction can

produce two key low energy products $HNO_3 + N_2H_3$ *via* the direct H-abstraction path with 1.2 kcal/mol barrier and t-HONO + $N_2H_3O$ *via* the concerted transfer of O and H atoms via a 5-member-ring intermediate with 3.1 kcal/mol negative barrier lying below the intermediate. The computed heats of formation $\Delta_f H_0^\circ$ at 0 K for $N_2H_3$, $H_2NNO$, $N_2H_3O$, 56.8, 19.5 and 37.8 kcal/mol, respectively, are in good agreement with experimental results. The rate constants for reactions occurring without intrinsic barriers (such as those in the $NO_3$ reactions and some reverse processes involving HNO and HONO) were evaluated with the variational transition state theory. Their rate constants have been calculated in the temperature range 300–2000 K by TST/VTST and/or RRKM theory with Eckart tunneling and multiple-reflection corrections.

## Acknowledgments

The authors deeply appreciate the support by Taiwan's National Science Council (NSC) under contract No. NSC100-2113-M-009-013 and by the Ministry of Education's ATU program. MCL also acknowledges the support from the NSC for the distinguished visiting professorship at National Chiao Tung University in Hsinchu, Taiwan. We are also grateful to the National Center for High-performance Computing for computer time and the use of its facilities.

## Appendix A. Supplementary material

Supplementary data associated with this article can be found, in the online version, at http://dx.doi.org/10.1016/j.comptc.2014.07.011.

## References

[1] P. Raghunath, N.T. Nghia, M.C. Lin, Ab Initio chemical kinetics of key processes in the hypergolic ignition of hydrazine and nitrogen tetroxide, Adv. Quantum Chem. 69 (2014) 253–301.
[2] R.F. Sawyer, I. Glassman, Gas-phase reactions of hydrazine with nitrogen dioxide and oxygen, Proc. Combust. Inst. 11 (1967) 861–869.
[3] K.-Y. Lai, R. Zhu, M.C. Lin, Why mixtures of hydrazine and dinitrogen tetroxide are hypergolic?, Chem Phys. Lett. 537 (2012) 33–37.
[4] A.M. Mebel, K. Morokuma, M.C. Lin, Modification of the Gaussian 2 theoretical model: the use of coupled cluster energies, density functional geometries, and frequencies, J. Chem. Phys. 103 (1995) 7414–7421.
[5] Y. Daimon, H. Terashima, M. Koshi, Evaluation of rate constants relavant to the hypergolic reaction of hydrazine with nitrogen dioxide, in: 7th Mediterranean Combustion Symposium, Chia Laguna, Cagliari, Sardinia, Italy, September 11–15, 2011.
[6] M.J. Frisch, G.W. Trucks, H.B. Schlegel, et al., in: Gaussian 09, Revision A.1, Gaussian, Inc., Wallingford CT, 2009.
[7] J.A. Pople, M. Head-Gordon, K. Raghavachari, Quadratic configuration interaction. A general technique for determining electron correlation energies, J. Chem. Phys. 87 (1987) 5968–5975.
[8] A.D. Becke, A new mixing of Hartree–Fock and local density-functional theories, J. Chem. Phys. 98 (1993) 1372–1377.
[9] A.D. Becke, Density functional thermochemistry. III. The role of exact exchange, J. Chem. Phys. 98 (1993) 5648–5652.
[10] T. Ishiwata, I. Tanaka, K. Kawaguchi, E. Hirota, Infrared diode spectroscopy of the $NO_3$ $\nu_3$ band, J. Chem. Phys. 82 (1985) 2196–2205.
[11] K.A. Peterson, D.E. Woon, T.H. Dunning Jr., Benchmark calculations with correlated molecular wave functions. IV. The classical barrier height of the $H + H_2 \rightarrow H_2 + H$ reaction, J. Chem. Phys. 100 (1994) 7410–7415.
[12] D.E. Woon, T.H. Dunning Jr., Gaussian basis sets for use in correlated molecular calculations. V. corevalence basis sets for boron through neon, J. Chem. Phys. 103 (1995) 4572–4585.
[13] S.J. Klippenstein, A.F. Wagner, R.C. Dunbar, D.M. Wardlaw, S.H. Robertson, VARIFLEX: Version 1.00, 1999.
[14] M.W.J. Chase, NIST-JANAF Thermochemical, Tables, fourth ed.; J. Phys. Chem. Ref. Data Monograph No. 9 (Parts I and II), 1998.
[15] M.H. Matus, A.J. Arduengo III, D.A. Dixon, The heats of formation of diazene, hydrazine, $N_2H_3^+$, $N_2H_5^+$, $N_2H$, and $N_2H_3$ and the methyl derivatives $CH_3NNH$, $CH_3NNCH_3$, and $CH_3HNNHCH_3$, J. Phys. Chem. A 110 (2006) 10116–10121.
[16] U. Wille, T. Dreessen, Mechanistic insights into $NO_3^\bullet$ induced self-terminating radical oxygenations, Part 1: a computational study on $NO_3^\bullet$ and its addition to alkynes, J. Phys. Chem. A 110 (2006) 2195–2203.
[17] Z.F. Xu, M.C. Lin, Computational studies on the kinetics and mechanisms for $NH_3$ reactions with $ClO_x$ ($x = 0$–4) radicals, J. Phys. Chem. A 111 (2007) 584–590.
[18] B. Ruscic, J.E. Boggs, A. Burcat, et al., IUPAC critical evaluation of thermochemical properties of selected radicals, Part I. J. Phys. Chem. Ref Data 34 (2005) 573–656.
[19] S. Glasstone, K.J. Laidler, H. Eyring, The Theory of Rate Processes, McGraw-Hill, New York, 1941.
[20] W.H. Miller, Tunneling corrections to unimolecular rate constants, with application to formaldehyde, J. Am. Chem. Soc. 101 (1979) 6810–6814.
[21] W.H. Miller, Unified statistical model for "complex" and "direct" reaction mechanisms, J. Chem. Phys. 65 (1976) 2216–2223.
[22] Z.F. Xu, C.-H. Hsu, M.C. Lin, Ab initio kinetics of the reaction of HCO with NO: abstraction versus association/elimination mechanism, J. Chem. Phys. 122 (2005) 234308.
[23] L.Y. Carl, Handbook of thermodynamic diagrams, first ed., William Andrew Publishing, US, 1996. vol. 4.